ISSN 0016-7932, Geomagnetism and Aeronomy, 2013, Vol. 53, No. 3, pp. 397–408. © Pleiades Publishing, Ltd., 2013.
Original Russian Text © N.P. Perevalova, A.S. Polyakova, A.I. Pogoreltsev, 2013, published in Geomagnetizm i Aeronomiya, 2013, Vol. 53, No. 3, pp. 414–426.

Variations in the Characteristics of Acoustic Gravity Waves according to Simulation Data

N. P. Perevalova[a], A. S. Polyakova[a], and A. I. Pogoreltsev[b]

[a] *Institute of Solar–Terrestrial Physics of Siberian Branch of Russian Academy of Sciences, P.O. Box 291, Irkutsk, 664033 Russia*

[b] *Russian State Hydrometeorological University, St. Petersburg, Russia*

e-mail: pereval@iszf.irk.ru

Received June 7, 2011; in final form, December 14, 2011

Abstract—The characteristics of different-scale acoustic gravity waves (wavelengths of 100–1200 km, periods of 10–50 min) under different geophysical conditions have been studied using a numerical model for calculating the vertical structure of these waves in a nonisothermal atmosphere in the presence of an altitude-dependent background wind and in a situation when molecular dissipation is taken into account. It has been established that all considered acoustic gravity waves (AGWs) effectively reach altitudes of the thermosphere. The character of the amplitude vertical profile depends on the AGW scales. The seasonal and latitudinal differences in the AGW vertical structure depend on the background wind and temperature. A strong thermospheric wind causes the rapid damping of medium-scale AGWs propagating along the wind. Waves with long periods to a lesser degree depend on dissipation in the thermosphere and can penetrate to high altitudes. A change in the geomagnetic activity level affects the background wind vertical distribution at high latitudes, as a result of which the AGW vertical structure varies.

DOI: 10.1134/S0016793213030146

1. INTRODUCTION

Much attention has recently been paid to studying the effect of tropospheric disturbances on ionospheric parameters. Such disturbances are caused by earthquakes, hurricanes, atmospheric fronts, etc. Acoustic gravity waves (AGWs) are among the main mechanisms by which disturbance energy is transmited from the troposphere to ionospheric altitudes. Therefore, it is interesting to study the penetration altitude of AGWs generated by near-Earth sources, as well as the AGW characteristics (period, wavelength, and phase velocity) necessary for these waves to cause pronounced disturbances of ionospheric parameters.

The background wind and the processes of molecular viscosity and thermal conductivity play a key role in the formation of the AGW vertical structure (Gossard and Hooke, 1975; Gavrilov, 1985; Bidlingmayer et al., 1990; Bidlingmayer and Pogoreltsev, 1992; Pogoreltsev and Pertsev, 1995; Akhmedov and Kunitsyn, 2004; Kunitsyn et al., 2007). At the same time, it is difficult to take into account the terms describing dissipation due to viscosity and thermal conductivity in hydrothermodynamic equations, since numerical implementation is complex. Therefore, viscosity and thermal conductivity are ignored (Gavrilov, 1985) or different parametrizations are used to describe the above effects when the AGW generation and propagation are numerically simulated. Researchers most frequently use the representation of molecular and turbulent viscosity in the form of the Rayleigh friction force $\mathbf{F} = -\alpha\mathbf{v}$ ($\mathbf{v}$ is the particle velocity, and α is dynamic viscosity (Landau and Lifshits, 1978)) and write the dissipative term for thermal conductivity as $Q = k\Delta T$ (T is temperature, and k is the air thermal conductivity) (Ivanovsky and Semenovsky, 1973; Akhmedov and Kunitsyn, 2004; Kunitsyn et al., 2007). A numerical model for calculating the AGW vertical structure in a nonisothermal atmosphere stratified with respect to density was developed in (Bidlingmayer and Pogoreltsev, 1992; Pogoreltsev and Pertsev, 1995) for a situation when an altitude-dependent background wind is present and molecular dissipation, caused by viscosity and thermal conductivity, is taken into account. The model's advantage consists in that the dissipative terms are taken into account explicitly, i.e., without parametrizations, which makes it possible to obtain a more realistic knowledge of the AGW structure at different altitudes. The aim of this work was to study the characteristics of different-scale AGWs, depending on the season, latitude, geomagnetic activity level, and source parameters, based on the indicated model.

2. MODEL OF THE AGW VERTICAL STRUCTURE

The numerical model of the AGW vertical structure (Bidlingmayer and Pogoreltsev, 1992; Pogoreltsev and Pertsev, 1995) is based on a set of hydrodynamic equations (motion, continuity, energy conservation, and perfect gas equations), which takes into account all terms describing viscous dissipation and molecular thermal conductivity. The initial set is linearized relative to an undisturbed background state (a windless nonisothermal atmosphere). Disturbances of the hydrodynamic parameters (pressure p', temperature T', and zonal (u') and meredional (w') wind velocities) are represented as plane monochromatic waves propagating along the x axis:

$$\frac{p'}{P(\xi)p_0} = \frac{T'}{T(\xi)T_0} = \frac{u'}{U(\xi)(g/\omega)} = \frac{w'}{W(\xi)(g/\omega)} = \exp(ik_x x - i\omega t), \quad (1)$$

where p_0 and T_0 are background pressure and temperature, respectively; $P(\xi)$, $T(\xi)$, $U(\xi)$, and $W(\xi)$ are the complex dimensionless amplitudes of pressure, temperature, and zonal and meridional wind velocity disturbances, respectively; ω and k_x are the frequency and horizontal projection of the AGW wave vector, respectively; g is the gravitational acceleration; $\xi = \int_0^z dz'/H_0(z')$ is the dimensionless height; $H_0 = RT_0/Mg$ is the height of a homogeneous atmosphere; R is the universal gas constant; and M is the air molecular weight. The hydrostatic and state equations are used for the background characteristics of the atmosphere: $p_0(\xi) = p_0(0)\exp(-\xi)$; $p_0 = RT_0\rho_0/M$. Molecular thermal conductivity and shear-viscosity coefficients are specified as follows (Bidlingmayer and Pogoreltsev, 1992): $k = k_0T_0^{2/3}/M$; $\mu_1 = 4k/[(9\gamma - 5)c_v]$, where $\gamma = c_p/c_v$; T_0 and M are expressed in Kelvin and atomic units, respectively; and $k_0 = 0.015$ J (K m s)$^{-1}$ is an empirically obtained constant. The calculations are performed for a nonisothermal atmosphere, taking into account vertical variations in M and γ. The ground level density $\rho_0(z = 0)$ and the background temperature profile $T_0(z)$ are calculated using the model from (Fleming et al., 1988) up to an altitude of 100 km. It is considered that M and γ are constant up to an altitude of 100 km: $M = 28.9$, and $\gamma = 1.4$. The MSIS-90 model (Hedin, 1991) is used to calculate the $T_0(z)$, $M(z)$, and $\gamma(z)$ vertical profiles above an altitude of 100 km. The (Fleming et al., 1988) empirical model and the (Hedin et al., 1991) model are used to obtain background wind profiles in the lower and middle atmospheres, respectively.

The source modeling excitation of AGWs enters into the motion equation for the horizontal wind velocity component and specifies the momentum disturbance, which is subsequently transferred to all hydrodynamic parameters. The expression for a source has the form

$$f' = ig\rho_0F_0\exp\left[-(z - z_i)^2/\Delta z^2\right]\exp(ik_x x - i\omega t), \quad (2)$$

where F_0, $2\Delta z$, and z_i are the source amplitude, vertical extension, and height, respectively.

The modified sweep method, which makes it possible to avoid difficulties related to the fact that the coefficients of higher derivatives are small at altitudes where dissipation becomes negligible, was proposed in order to numerically solve the obtained set of equations (Bidlingmayer and Pogoreltsev, 1992; Pogoreltsev and Pertsev, 1995). The method is based on the fact that the dissipative solution changes into the classical solution for waves without dissipation with decreasing altitude. The $\varepsilon = \mu_1/[\omega\rho_0H_0^2]$ parameter was selected as a criterion for separating regions with different solutions. In the lower atmosphere, where molecular dissipation can be neglected, $\varepsilon \ll 1$ (the classical region); in the upper atmosphere, where dissipative processes are decisive, $\varepsilon \gg 1$ (the dissipative region). During calculations, a peculiar solution is constructed for either region and the obtained solutions are coupled at the boundaries between the regions. The boundary between the classical and dissipative regions is at altitudes of 80–100 km.

As a result of the calculations, the model gives amplitude and phase vertical profiles for all complex values $P(z)$, $T(z)$, $U(z)$, and $W(z)$, which characterize wave-like disturbances of the hydrodynamic parameters with a specified frequency and horizontal wavelength.

3. VERTICAL STRUCTURE OF STEADY-STATE AGWs

To study the AGW structure in the thermosphere using the model in (Bidlingmayer and Pogoreltsev, 1992; Pogoreltsev and Pertsev, 1995), we calculated the vertical profiles of the amplitude and phase of fluctuations in the atmospheric hydrodynamic parameters, taking into account the background wind, temperature, molecular thermal conductivity, and viscosity. The calculations were performed for day 15 of each month in 2005 at a longitude of 270° E at 0100 UT (1900 LT).

When test simulations were performed for model approbation, the source amplitude (F_0) was selected arbitrary and the calculation results were normalized so that the wave action vertical flux at an altitude of 100 km would be 5×10^{-5} J m^{-2} s^{-1} (Bidlingmayer and Pogoreltsev, 1992; Pogoreltsev and Pertsev, 1995). The wave action flux was determined so that its dimensionality would coincide with the energy flux dimensionality: $S = F/\tilde{\omega}$, where $\mathbf{F}$ is the energy flux, $\tilde{\omega} = (\omega - k_xu_0)/\omega$ is the dimensionless frequency, and u_0 is the velocity of the background zonal wind. The results described in this section were achieved using the above regime. We selected the following source parameters: $z_i = 10$ km, $\Delta z = 4$ km, and $F_0 = 10^{-4}$.

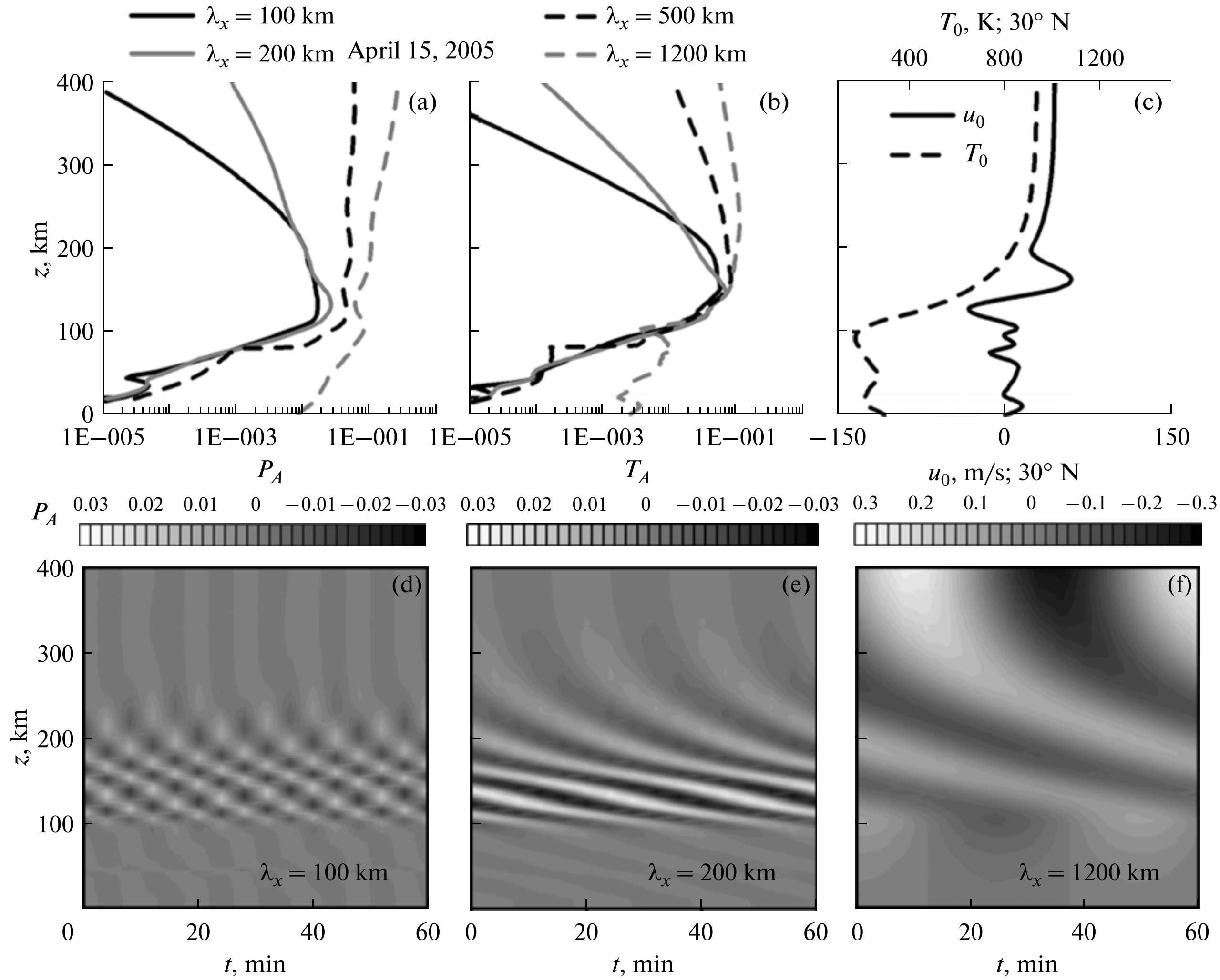

Fig. 1. Vertical profiles at a latitude of 30° N for April 15, 2005: the amplitudes of AGWs with wavelengths of 100, 200, 500, and 1200 km in variations in (a) pressure, (b) temperature, and (c) the background zonal wind velocity (u_0) and background temperature. The positive zonal wind is eastward. The altitude-time disturbances of the atmospheric pressure for AGWs with wavelengths of (d) 100 km, (e) 200 km, and (f) 1200 km.

3.1. Different-Scale AGW Penetration Altitudes

First of all, we analyzed the dependence of the altitude to which an AGW propagates on the wave scales (horizontal wavelength λ_x and period τ). For this purpose, we calculated the vertical profiles of four AGWs with the following characteristics: wavelength $\lambda_x = 100$ km, period $\tau \approx 10$ min; $\lambda_x = 200$ km, $\tau \approx 20$ min; $\lambda_x = 500$ km, $\tau \approx 30$ min; and $\lambda_x = 1200$ km, $\tau \approx 50$ min. The AGW parameters were selected based on experimental data on the average characteristics of traveling ionospheric disturbances (TIDs). It is considered that TIDs are ionospheric manifestations of AGWs. The calculations were performed for April 15, 2005, at a latitude of 30° N. It was assumed that AGWs propagate eastward (the horizontal phase velocity $V_x > 0$). The calculated profiles of the wave-like disturbance amplitude with the above characteristics in the pressure and temperature variations are shown in Figs. 1a and 1b. Figure 1c presents the profiles of the background wind velocity (u_0) and background temperature (T_0) for April 15, 2005. Figures 1d–1f present the distributions of pressure disturbances relative to the background level caused by waves with $\lambda_x = 100$, 200, and 1200 km. According to expression (1), pressure disturbances have the form $p'(t, z)/p_0 = P_A(z)\cos[\omega t - P_\varphi(z)]$, where p'/p_0 is the value of pressure deviations from the undisturbed level and ω, P_A, and P_φ are the AGW frequency, amplitude, and phase, respectively.

Figure 1a indicates that the amplitudes of waves with $\lambda_x = 100$ and 200 km have a maximum at an altitude of ~120 km. The waves start damping above an altitude of 120 km and almost disappear at altitudes of 380–400 km. Pressure deviations from the background level, caused by these AGWs at thermospheric

Table 1. Values of the Ap and $F10.7$ indices in 2005

Date	Ap	$F10.7$	Date	Ap	$F10.7$
January 15	18	140.2	July 15	4	90.1
February 15	4	118.7	August 15	6	77.7
March 15	4	107.0	September 15	52	120.6
April 15	13	85.5	October 15	2	79.1
May 15	87	105.2	November 15	4	97.8
June 15	16	97.5	December 15	2	84.2

altitudes, are no more than 3%. The amplitude of large-scale waves (λ_x = 500 and 1200 km) also increases to an altitude of ~120 km; however, above this level, these waves do not break with increasing altitude. Large-scale AGWs can cause disturbances of the pressure field at thermospheric altitudes, reaching 10%. The character of the altitudinal dependences of temperature wave disturbances with λ_x = 100 and 200 km (Fig. 1b) is generally similar to the disturbance amplitude profile. However, the maximal amplitudes in temperature are slightly larger than such amplitudes in pressure and reach 5–6%. The temperature maximum is formed at a higher altitude (~150 km). In contrast to pressure disturbances, large-scale temperature disturbances (λ_x = 500 and 1200 km) damp in the thermosphere (although rather slowly), and the values of their maximal amplitude are close to those of small-scale AGWs.

Thus, a comparison of the AGW model profiles indicated that waves with long periods and wavelengths have larger amplitudes, are less subjected to dissipation, and can penetrate to higher altitudes. Below 50–70 km, the calculated AGW amplitudes are small. The amplitude increases rapidly at altitudes of 70–130 km. The further amplitude behavior depends on the AGW scales: small-scale waves have an amplitude maximum at altitudes of 120–130 km, and the amplitude of large-scale AGWs in the 130–400 km interval changes insignificantly with increasing altitude. The obtained results agree with the conclusions made in (Bidlingmayer and Pogoreltsev, 1992; Pogoreltsev and Pertsev; 1995) and with the results of the model calculations in (Gavrilov and Yudin, 1986; Akhmedov and Kunitsyn, 1986; Kunitsyn et al., 2007). Gavrilov and Yudin (1986) indicated that AGWs with a horizontal phase velocity of 150 km/s have an amplitude maximum at an altitude of 125 km. Amplitudes of $|T/T_0|$ ~ 4.5–5% were obtained in the maximum region. The calculations, performed in (Akhmedov and Kunitsyn; Kunitsyn et al., 2007) for an isothermal atmosphere, indicated that AGWs caused by surface pulsed sources have the maximal amplitude at an altitude of ~150 km (the horizontal phase velocities of AGWs were ~200 m/s, and the periods reached 1000 s).

3.2. Amplitude of Medium-Scale AGWs

The vertical profiles of medium-scale ($\tau \approx$ 20 min, λ_x = 200 km, and horizontal phase velocity $V_x \approx$ 160 m/s) and large-scale ($\tau \approx$ 50 min, λ_x = 1200 km, and $V_x \approx$ 400 m/s) waves at two latitudes (30° and 60° N) were obtained for the 15th day of each month in 2005 in order to study the dependence of the AGW parameters on the season, latitude, and background conditions. The eastward ($V_x > 0$) and westward ($V_x < 0$) waves were considered in all cases. The Ap and $F10.7$ (solar radioemission flux) indices (ftp://ftp.dmi.dk/pub/Data/WDCC1/indices) were used to specify the geophysical conditions during modeling. The values of these parameters are presented in Table 1.

Figure 2 (left) presents the vertical profiles of the medium-scale AGW amplitude in March, June, September, and December 2005 at latitudes of 30° (solid lines) and 60° N (dashed lines). The amplitudes of eastward ($V_x > 0$) and westward ($V_x < 0$) AGWs are marked in black and gray, respectively. The vertical profiles of background zonal wind u_0 (solid lines) and temperature T_0 (dashed lines) on the days for which AGWs were modeled are presented in the central and left-hand columns in Fig. 2 (for latitudes of 30° and 60° N, respectively). According to Fig. 2, medium-scale AGWs effectively reach thermospheric altitudes, independently of the wind velocity and direction in the stratosphere and mesosphere. The AGW amplitude vertical profiles have a characteristic maximum at altitudes of 100–150 km, above which waves dissipate. Westward and eastward AGWs have close amplitudes at altitudes up to ~100 km, independently of the latitude and season. At the same time, an exponential increase in the AGW amplitude in this region of altitudes is often disturbed by local maximums (minimums), apparently caused by wave reflection from regions with steep background wind gradients.

In the dissipative region (z > 100 km), seasonal and latitudinal differences in the AGW amplitude altitudinal behavior are caused by the background wind and temperature. Systematic differences in the behavior of waves propagating along and against the wind are observed in this case.

The weakest wind in the entire considered atmosphere was observed on September 15 at a latitude of 30° N (Fig. 2h). The wind velocity in the thermosphere was close to zero on that day. In this case, the minimal difference in the vertical profiles of westward and eastward AGWs was registered at this latitude (Fig. 2g). A similar pattern was observed on June 15 (Figs. 2d, 2e) and May 15 at a latitude of 30° N, as well as on February 15, March 15 (Figs. 2a, 2c), August 15, November 15, and December 15 (Figs. 2k, 2m) at a latitude of 60° N. However, the background wind velocity on those days was slightly higher than on September 15, which probably resulted in larger differences in the vertical profiles of two types of AGWs at z > 150 km.

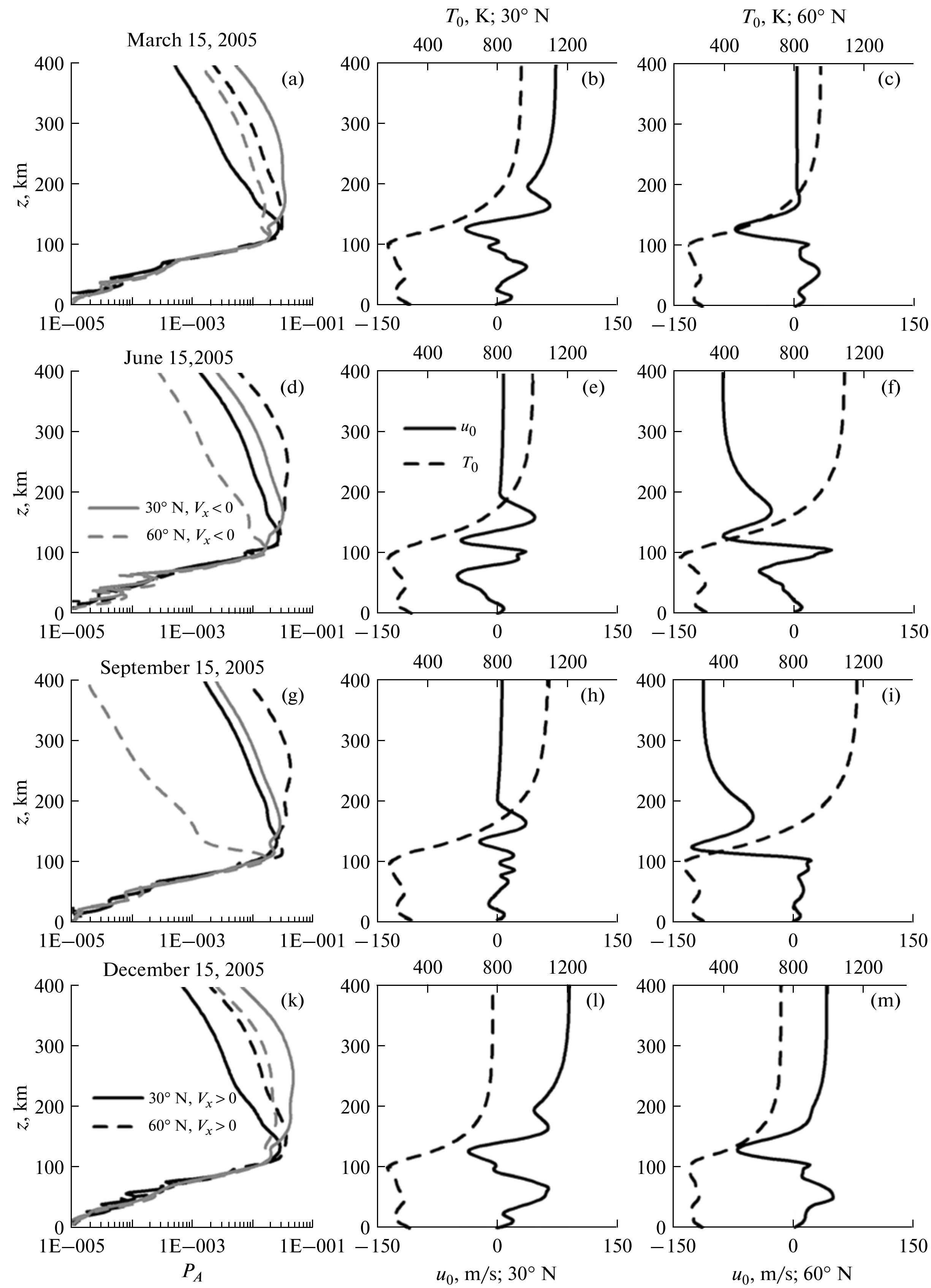

Fig. 2. Vertical amplitude profiles (P_A) of medium-scale AGWs, background zonal wind velocity (u_0), and background temperature (T_0) in (a–c) March, (d–f) June, (g–i) September, and (k–m) December at latitudes of 30° and 60° N. The positive zonal wind is eastward.

Higher (>100 m/s) background zonal wind velocities at the thermospheric altitude were registered at a latitude of 60° N (Fig. 2i). The wind was westward. Under these conditions, the westward wave ($V_x < 0$) weakened rapidly at altitudes $z > 150$ km at a latitude of 60° N (Fig. 2g). The AGW, which propagated downwind, almost completely broke at an altitude of about 250 km. The maximal amplitude of this AGW and the altitude at which the wave starts damping also decreased. An opposite pattern was observed for an AGW that propagated eastward (upwind, $V_x > 0$). The amplitude of this wave increased and remained unchanged at altitudes of 120–250 km. The wave started dissipating only above a altitude of 250 km.

A similar situation was formed on May 15, 2005. On that day, the westward wind velocity in the thermosphere was higher than 150 m/s at a latitude of 60° N, as a result of which the AGW profiles were cardinally changed. The wave that propagated downwind ($V_x < 0$) almost dissipated at an altitude of ~170 km. The amplitude of the wave that propagated upwind ($V_x > 0$) increased up to an altitude of ~260 km. On March 15 (Fig. 2b) and December 15 (Fig. 2k), considerable velocities of the eastward zonal wind were observed at a latitude of 30° N. This resulted in the weakening of AGWs that propagated eastward (downwind) and in the amplification of oppositely directed waves at altitudes $z > 150$ km (Figs. 2a, 2k). Similar, but less pronounced, amplification (weakening) effects of altitudinal dissipation of eastward (westward) waves (since the thermospheric wind velocity was lower) were observed in all considered cases. At altitudes of ~200 km, the pressure fluctuations caused by waves propagating downwind is no more than 1% of the background level. Oppositely directed AGWs result in pressure deviations from the background value, reaching 5–6%. Large deviations remain at altitudes of 100–300 km. We note that maximal disturbances of the pressure field are registered at an altitude of the main ionospheric maximum (250–300 km). Thus, the zonal thermospheric wind causes a decrease in the maximal amplitude and maximum altitude of AGWs propagating downwind, as well as the rapid damping of these waves at altitudes $z > 150$ km. The amplitude of waves propagating upwind increases, the altitude at which such AGWs start damping also pronouncedly increases, and such waves dissipate substantially slower with increasing altitude.

The described specific features in the behavior of waves propagating in opposite directions correspond to the results achieved in (Pogoreltsev and Pertsev, 1995): in the example presented by the authors, AGWs moving upwind also have a high maximum altitude and a large amplitude at altitudes $z > 100$ km. The possible causes of the observed phenomena are discussed in detail in Subsection 3.4.

The anomalous vertical distribution of the background wind and temperature at a latitude of 60° N, which was observed on January 15, May 15, June 15, and September 15, 2005, was caused by an increased geomagnetic activity on those days. According to Table 1, the magnetic activity level on January 15 and June 15, 2005 (Ap = 16–18), was increased as compared to the quiet level (Ap = 2–4). At the same time, moderate magnetic storms were observed on May 15 (Ap = 87) and September 15 (Ap = 52). Thus, a change in the geomagnetic activity level largely changes the background wind vertical distribution at high latitudes and near them and, as a consequence, transforms the AGW structure.

3.3. Amplitude of Large-Scale AGWs

The calculations of the amplitude profiles of large-scale AGWs ($\tau \approx 50$ min, $\lambda_x = 1200$ km, and $V_x \approx 400$ m/s) are illustrated in Fig. 3 in a format similar to Fig. 2. Long-period AGWs, as well as medium-scale waves, effectively penetrate to thermospheric altitudes independently of the wind velocity and direction in the stratosphere and mesosphere. This agrees with the modeling results, which indicated that AGWs with a horizontal wavelength larger than 50 km and with a high horizontal phase velocity almost always reach altitudes of the lower thermosphere (Preusse et al., 2008). The vertical profiles of large-scale AGWs have no pronounced maximum: the wave amplitude generally increases with increasing altitude, which indicates that these AGWs weakly dissipate in the thermosphere. At altitudes of 100–200 km, the profiles are undulating and have one or two local maximums, possibly related to partial reflections from regions with strong background wind and temperature nonuniformities. In the lower atmosphere (0–50 km altitudes), the amplitude of large-scale AGWs is three orders of magnitude as large as that of medium-scale waves. At altitudes of 100–150 km, where the medium-scale wave maximum is observed, the amplitude of large-scale AGWs is larger by a factor of 2–3.

The seasonal and latitudinal differences in the amplitude vertical profiles of long-period waves are very imperceptible, which indicates that these profiles weakly depend on the background characteristics of the atmosphere. The differences in the wind and temperature vertical distribution at latitudes of 30° and 60° N are substantial; nevertheless, the AGW amplitude has close values and identical vertical variations at these latitudes. Pronounced differences in the amplitude behavior below an altitude of 100 km for westward and eastward AGWs were registered in the summer months (May–August), when the background wind values at altitudes of 70–200 km are large. In this case, eastward waves intensify (Figs. 3d, 3f). The damping of large-scale waves in the thermosphere depends less on the propagation direction than that of medium-scale waves. On days when the background wind value in the upper thermosphere is not larger than 50 m/s (e.g., on March 15 (Figs. 3a, 3c) and December 15 (Figs. 3j, 3l)

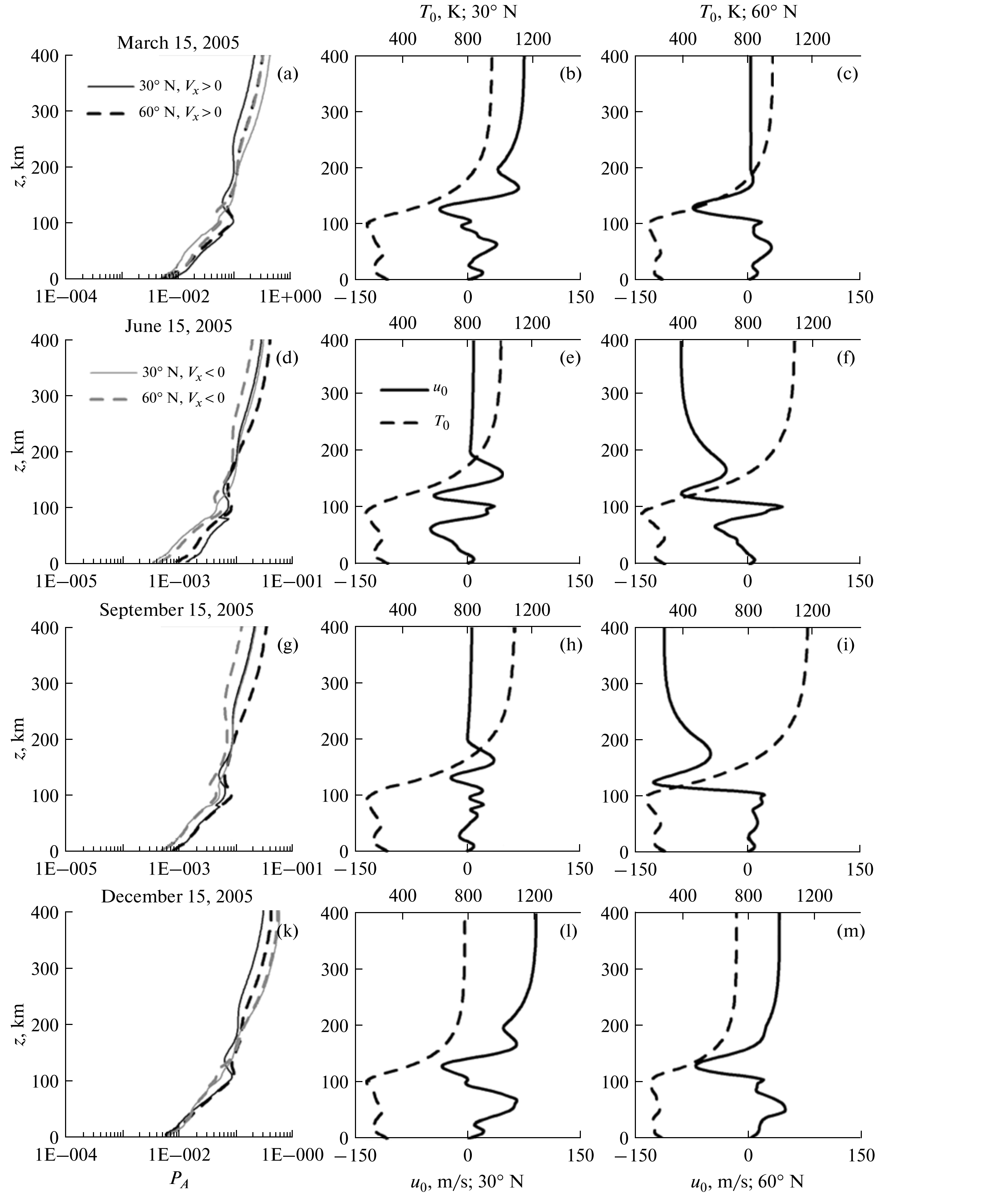

Fig. 3. Vertical amplitude profiles (P_A) of large-scale AGWs, background zonal wind velocity (u_0), and background temperature (T_0) in (a–c) March, (d–f) June, (g–i) September, and (k–m) December at latitudes of 30° and 60° N. The positive zonal wind is eastward.

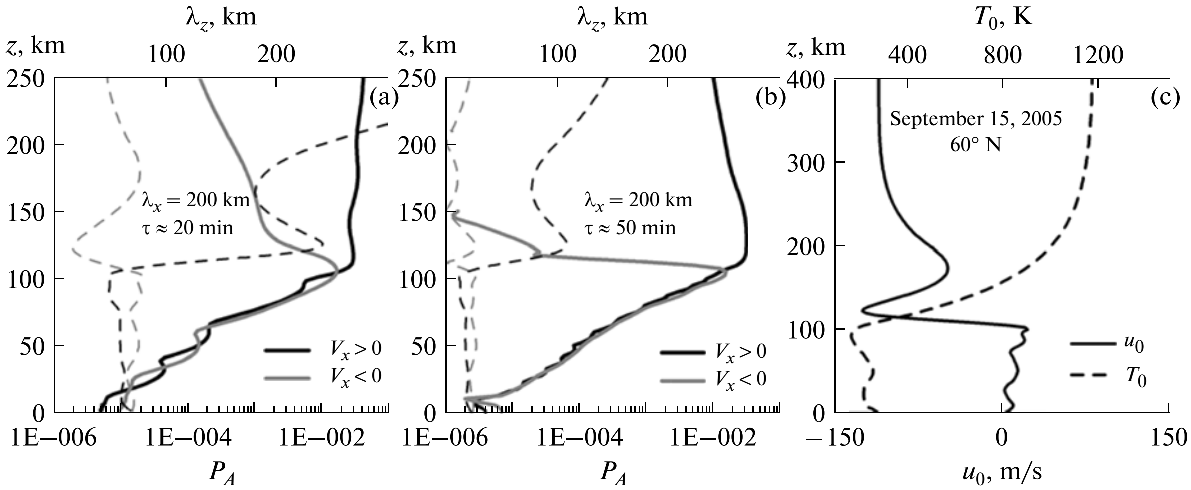

Fig. 4. Vertical amplitude profiles of AGWs with a wavelength of 200 km and periods of (a) $\tau \approx 20$ and (b) $\tau \approx 50$ min, propagating toward east ($V_x > 0$) and west ($V_x < 0$), and (c) the zonal wind velocity (u_0) and temperature (T_0) at a latitude of 60° N for September 15, 2005.

at a latitude of 60° N and June 15 (Figs. 3d, 3e) at a latitude of 30° N), the amplitude profiles of large-scale westward and eastward AGWs at $z > 150$ km almost coincide. During geomagnetic disturbances (May 15 and September 15, see Figs. 3g, 3i), when a strong westward wind exists in the thermosphere, the amplitudes of eastward waves ($V_x > 0$) are larger by a factor of 1.5–2. However, the vertical profile character is the same as such a character for oppositely directed waves. Thus, AGWs with large wavelengths and high phase velocities depend less on the background characteristics of the atmosphere. This corresponds to the results obtained in (Pogoreltsev and Pertsev, 1995), who noted that the effectiveness of AGW penetration into the upper thermosphere depends less on the propagation direction with increasing horizontal wavelength.

3.4. Factors Affecting the AGW Vertical Structure

The amplification of AGWs propagating upwind and the attenuation of waves propagating downwind can be explained by the wave Doppler frequency shift. The calculated vertical structure and the value of the AGW amplitude are affected by three factors dependent on the wave frequency: dissipation, reflection, and normalization used in the model. The Doppler shift results in an increase in the frequency and, as a consequence, in an increase in the vertical wavelength of AGWs propagating upwind. For waves moving downwind, the frequency and λ_z decrease. The dashed lines in Fig. 4a show the λ_z values for medium-scale waves ($\lambda_x = 200$ km, $\tau \approx 20$ min, and $V_x \approx 160$ m/s), propagating eastward ($V_x > 0$) and westward ($V_x < 0$) on September 15 at a latitude of 60° N. The vertical profiles of the background wind and temperature on that day are shown in Fig. 4c. The vertical wavelength of an AGW, moving upwind ($V_x > 0$) at thermospheric altitudes, is substantially longer than that of a wave directed downwind ($V_x < 0$). This fact is confirmed by the model calculations performed in (Gavrilov and Yudin, 1986; Pogoreltsev and Pertsev, 1995). Short-wavelength disturbances are more strongly subjected to dissipation than long-wavelength ones (Yanowitch, 1967; Ivanovsky and Semenovsky, 1973; Gavrilov and Yudin, 1986; Pogoreltsev and Pertsev, 1995). Therefore, a strong wind attenuates following waves. To verify the achieved result, we calculated the amplitude vertical profile of an AGW with a frequency lower by a factor of 2.5 ($\lambda_x = 200$ km, $\tau \approx 50$ min, and $V_x \approx 67$ m/s). The calculation results are shown in Fig. 4b, which indicates that the wave that propagated downwind had very small λ_z values and almost completely dissipated at an altitude of ~150 km.

On the other hand, the AGW downward reflection from the thermosphere increases with increasing vertical wavelength (Yanowitch, 1967; Ivanovsky and Semenovsky, 1973). Figures 4a and 2 indicate that reflections are present for the ($\lambda_x = 200$ km, $\tau \approx 20$ min) wave. In the absence of reflections below the dissipative region ($z < 100$ km), the wave amplitude on the logarithmic scale should linearly vary with increasing altitude. Such a behavior is typical of the ($\lambda_x = 200$ km, $\tau \approx 50$ min) wave, which has short λ_z (Fig. 4b). The profiles of the medium-scale AGW amplitude at altitudes of 0–100 km (Figs. 4a, 2) are undulating, which is caused by partial wave reflection from the dissipative region and from regions with large background wind and temperature gradients. The presence of reflection should generally result in a decrease in the wave amplitude in the thermosphere. However, the normalization with respect to the wave action vertical flux used in the model normalize the total (up and down) flux.

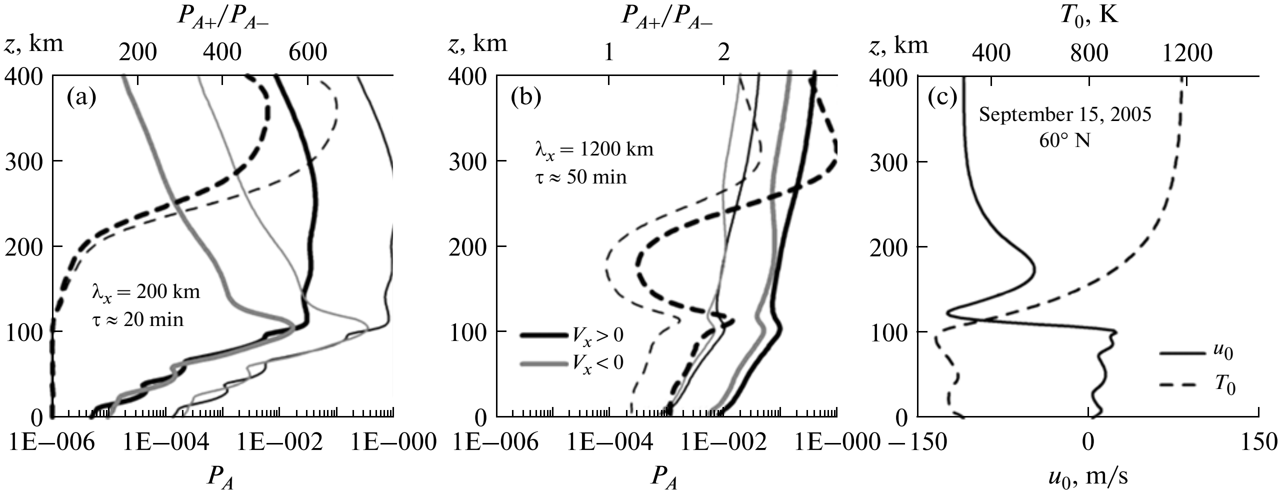

Fig. 5. Vertical amplitude profiles of AGWs with (a) $\lambda_x = 200$ km and $\tau \approx 20$ min and (b) $\lambda_x = 1200$ km and $\tau \approx 50$ min, propagating toward east ($V_x > 0$) and west ($V_x < 0$), and (c) the zonal wind velocity (u_0) and temperature (T_0) at a latitude of 60° N for September 15, 2005. Dashed lines in panels (a) and (b) show the ratio of the amplitudes of eastward (P_{A+}) and westward (P_{A-}) AGWs. The profiles were calculated with (thick curves) and without (thin curves) normalization.

In the presence of a reflected wave, this will result in an increase in the amplitude of an AGW penetrating into the thermosphere.

Normalization with respect to the wave action vertical flux can also affect the value of the AGW amplitude. To study the dependence of the amplitude on the wave action flux, we calculated the vertical structure of the medium- ($\lambda_x = 200$ km, $\tau \approx 20$ min, and $V_x \approx 160$ m/s) and large-scale ($\lambda_x = 1200$ km, $\tau \approx 50$ min, and $V_x \approx 401$ m/s) AGWs that propagated eastward ($V_x > 0$) and westward ($V_x < 0$). The calculations were performed for September 15, 2005, at a latitude of 60° N (Fig. 5). In Figs. 5a and 5b, the profiles calculated taking into account and ignoring normalization are shown by thick and thin lines, respectively. The amplitudes are normalized using the coefficient proportional to the wave action flux at an altitude of 100 km: $F_{osq} = \sqrt{[\omega F_{100}]/[F_{norm}(\omega - k_x u_0)]}$, where F_{100} is the energy flux at an altitude of 100 km and $F_{norm} = 5 \times 10^{-5}$. According to the definition, F_{osq} will be larger for waves propagating along the wind. In the calculations without normalization, it was assumed that $F_{osq} = 1$.

For the conditions of September 15, 2005, the background wind velocity at an altitude of 100 km is $u_0 > 0$. Therefore, the normalization coefficient for the eastward waves was larger than for the waves that moved westward ($F_{osq+} > F_{osq-}$). For a medium-scale AGW, $F_{osq+} = 26.6$ and $F_{osq-} = 20.2$. The amplitudes of medium-scale AGWs decreased substantially as a result of normalization. In this case, the amplitude (P_{A+}) of the eastward wave decreased stronger. For a large-scale AGW, $F_{osq+} = 0.107$ and $F_{osq-} = 0.137$. Therefore, the amplitudes of large-scale waves increased after normalization. Thus, the normalization used in the model pronouncedly affects the value of the AGW amplitude, the character of the amplitude vertical variations remaining almost unchanged in this case.

3.5. Comparison with Experimental Data

Numerous experimental data of internal gravity wave (IGW) observations, performed using different methods, were accumulated at the IFA RAN stations located near Zvenigorod, Moscow region (Krasovsky et al., 1978; Grachev et al., 1981; Shefov et al., 2006). A network of spaced microbarographs was used to register IGWs in pressure variations (Grachev et al., 1981). According to the results obtained in (Grachev et al., 1981), the pressure amplitudes in the surface layer for IGWs with periods of 5–20 min can on average be 10–100 bar (1–10 Pa). Taking into account that the normal ground-level pressure is $p_0 \approx 1$ bar (101.325 kPa), we can state that the relative pressure wave amplitude should be 10^{-5}–10^{-4}. The amplitudes of AGWs in the ground-level pressure, calculated using the model in (Bidlingmayer and Pogoreltsev, 1992; Pogoreltsev and Pertsev, 1995), are slightly smaller: 5×10^{-6}–10^{-5}.

Nightglow emission observations (Krasovsky et al., 1978; Shefov et al., 2006) are used to study IGWs in the upper atmosphere at the Zvenigorod scientific station (geographic coordinates 55.7° N, 36.8° E) of the IFA RAN. Electrophotometers with interference filters make it possible to register the hydroxyl emission intensity, which is used to calculate the hydroxyl rotational temperature. It was indicated in (Krasovsky et al., 1978; Shefov et al., 2006) that the layer emitting hydroxyl is located at altitudes of ~90 km and has a thickness of ~10 km. The registered temperature is the vertically average layer temperature. It was also estab-

Table 2. Experimental and model amplitudes of temperature fluctuations with different periods at altitudes of 90–100 km

Period τ, min	Amplitude A_{av}, K	Rel. amplitude A'_{av}	Rel. amplitude T_A
10	4.6	0.02	0.003
20	8.2	0.043	0.004
30	8.6	0.043	0.005
40	10.1	0.051	–
50	13.1	0.063	0.005
60	20.3	0.097	0.007
70	15.6	0.077	–
80	19.4	0.103	–
90	25.4	0.118	–
100	26.1	0.123	–
120	26.2	0.14	0.01

lished that the hydroxyl rotational temperature reflects the ambient temperature. Krasovsky et al. (1978) presented the periods and amplitudes of temperature variations, as well as the average background temperatures (T_0) in the emitting layer, for many cases when IGWs were registered in 1973–1976.

Using the data presented in (Krasovsky et al., 1978), we calculated the average amplitudes of IGWs with periods of 10, 20, ..., 120 min, which are experimentally observed at altitudes of 90–100 km. The results are presented in the left part of Table 2 (τ is the IGW period; A_{av} and $A'_{av} = A_{av}/T_0$ are the average and average relative amplitudes of IGWs with period, calculated using the data in (Krasovsky et al., 1978)). The amplitudes (T_A) of temperature wave-like disturbances at altitudes of 90–100 km, calculated using the model in (Bidlingmayer and Pogoreltsev, 1992; Pogoreltsev and Pertsev, 1995) and normalization of the wave-action vertical flux at an altitude of 100 km described above, are presented in the right-hand column of Table 2. The model calculations were performed for April 15, 2005, at a latitude of 55° N and a longitude of 37° E (0300 LT). The level of magnetic and solar activity in April 2005 was the closest to such a level during experimental observations in 1973–1976. The point coordinates correspond to the position of the Zvenigorod station. Local time was selected, taking into account the fact that the experimental measurements were performed at night. A comparison of the experimental and model data in Table 2 indicates that the model gives temperature fluctuation amplitudes at altitudes of 90–100 km decreased by an order of magnitude. In this case, the model background temperatures in the above range of altitudes are close to the experimental values. When comparing, we should take into account the fact that waves are as a rule superposed in experiments. When the observed wave packet is resolved into individual harmonics, the amplitudes of these harmonics can be substantially smaller. At the same time, this decrease is sometimes related to the used normalization of the wave action flux at an altitude of 100 km (see Subsection 3.4). A change in the normalization value (F_{norm}) results in a corresponding change in the amplitude and can be used to coordinate model and experimental data. However, our calculations indicated that the vertical structure of steady-state AGWs is independent of the source parameters when normalization is used. Therefore, it seems reasonable to subsequently avoid normalization and select a disturbance source based on agreement between the amplitude of fluctuations caused by this source and experimental data.

4. EFFECT OF SOURCE PARAMETERS ON THE AGW VERTICAL STRUCTURE

To elucidate the effect of the disturbance source parameters on the AGW vertical structure in the (Bidlingmayer and Pogoreltsev, 1992; Pogoreltsev and Pertsev, 1995) model, we eliminated the normalization of the wave action flux at a altitude of 100 km and calculated the AGW amplitude and phase vertical profiles for different z_i, Δz, and F_0 values (see Section 2). The calculation results for a medium-scale wave ($\tau \approx 20$ min, $\lambda_x = 200$ km, and $V_x \approx 160$ m/s) at a latitude of 30° N on September 15 (the weakest zonal wind was observed at this latitude in the entire atmosphere on that day) are presented in Fig. 6.

As one would expect, an increase in the source amplitude results in a proportional increase in the amplitude of disturbances caused by this source (Figs. 6a, 6d). When the source intensity is $F_0 = 2 \times 10^{-5}$, the AGW amplitudes are the closest to the experimental data (Table 2). The average amplitude (T_A) of temperature fluctuations at altitudes of 90–100 km at $F_0 = 2 \times 10^{-5}$ is 0.023. Atmospheric gravity waves with the maximal amplitude are generated by a source with a vertical half-thickness of $\Delta z \sim 15$ km (Figs. 6b, 6e). The wave amplitude decreases slightly when the source half-thickness decreases and increases. When the source altitude (z_i) increases, the amplitude of disturbances caused by this source decreases (Figs. 6c, 6f). Sources at altitudes $z_i \sim 5$–30 km cause the formation of AGWs with rather close amplitudes. At $z_i > 30$ km, the amplitude decreases very rapidly with increasing z_i.

Thus, according to the preliminary modeling results, maximal disturbances are caused by AGWs, the sources of which have a large amplitude and vertical half-thickness $\Delta z \sim 15$ km and is located below 30 km altitude.

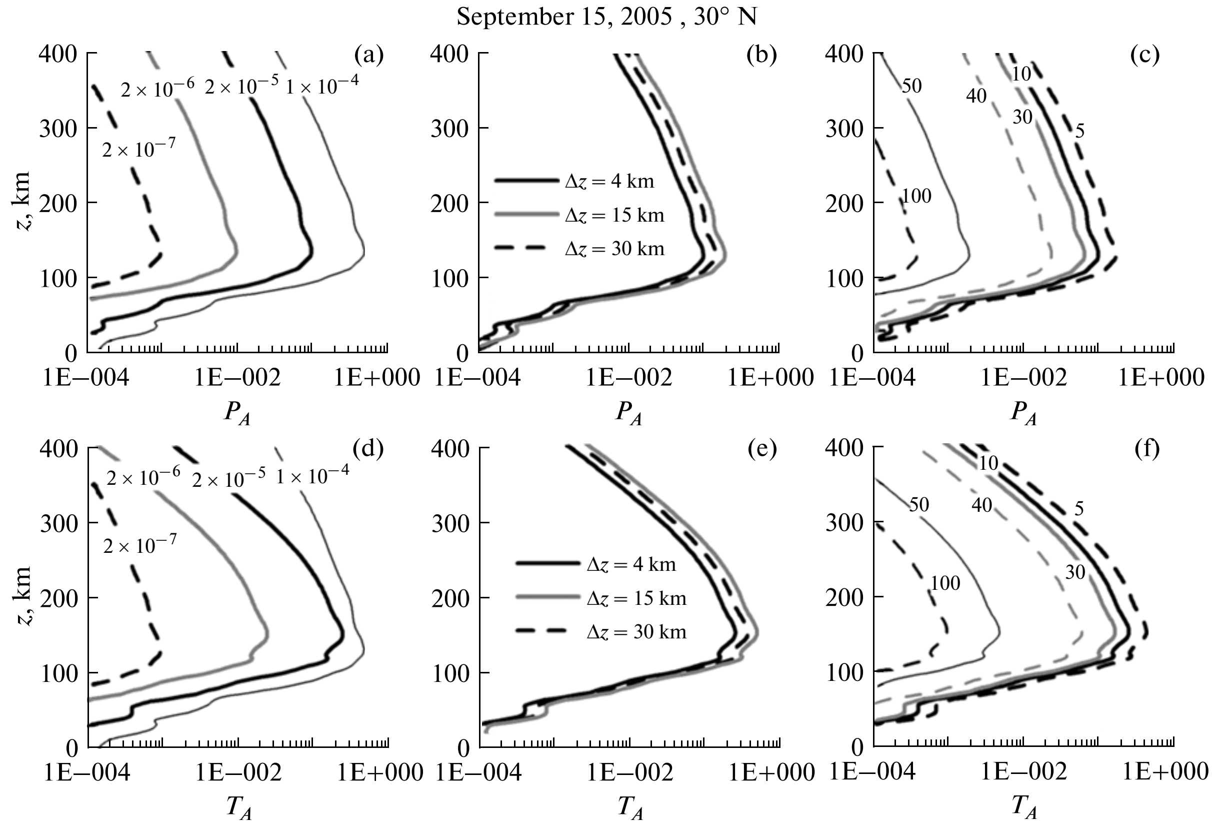

Fig. 6. Vertical amplitude profiles of (a–c) pressure and (d–f) temperature disturbances of medium-scale AGWs at different disturbance source parameters: (a, d) $z_i = 10$ km, $\Delta z = 4$ km, $F_0 = 1 \times 10^{-4}$, 2×10^{-5}, 2×10^{-6}, and 2×10^{-7}; (b, e) $z_i = 10$ km, $\Delta z =$ 4, 15, 30 km, $\Delta z = 30$ km, and $F_0 = 2 \times 10^{-5}$; and (c, f) $z_i = 5$, 10, 30, 40, 50, 100 km, $\Delta z = 4$ km, and $F_0 = 5 \times 10^{-5}$ (the z_i values are shown with numerals near curves).

5. CONCLUSIONS

We studied the different-scale AGW characteristics under different geophysical conditions, using a numerical model for calculating the AGW vertical structure in a nonisothermal atmosphere stratified with respect to density in the presence of the altitude-dependent background wind in a situation when molecular dissipation related to viscosity and thermal conductivity is taken into account (Bidlingmayer and Pogoreltsev, 1992; Pogoreltsev and Pertsev, 1995).

Medium- and long-period AGWs, calculated using the above model, identically effectively reach thermospheric altitudes independently of the background wind velocity and direction. We established that waves with long periods and wavelengths have large amplitudes, are less subjected to dissipation, and can penetrate to high altitudes. The amplitude of large-scale AGWs increases to an altitude of ~120 km, after which it changes slightly with increasing altitude. The amplitudes of medium-scale fluctuations below 50–70 km are small. The maximum of these AGWs is observed at altitudes of 120–130 km.

Seasonal and latitudinal differences in the vertical distributions of the AGW amplitude are caused by the background wind and temperature. The dependence on the AGW propagation direction is most pronounced for medium-scale waves and is related to the background zonal wind. Strong wind in the thermosphere causes a decrease in the maximum height and the maximal amplitude of AGWs that propagated downwind, as well as the rapid damping of these waves above an altitude of 150 km. The waves that propagated upwind had substantially larger calculated maximum amplitudes and heights and slower dissipated with increasing altitude. Seasonal and latitudinal differences in the vertical structure of long-period waves are imperceptible. The damping of large-scale waves in the thermosphere is less dependent on the propagation direction than that of medium-scale waves. When the thermospheric wind is strong, the amplitudes of waves moving upwind are larger by a factor of 1.5–2, but the vertical profile character is the same as for oppositely directed waves. Thus, AGWs with long wavelengths are less subjected to the effect of background atmospheric characteristics.

A change in the geomagnetic activity level affects the background wind vertical distribution at high latitudes, as a result of which the AGW vertical structure changes.

According to the preliminary results, maximal disturbances in the atmosphere are caused by AGWs, the sources of which have a large amplitude and vertical half-thickness $\Delta z \sim 15$ km and are located below an altitude of 30 km.

ACKNOWLEDGMENTS

This work was supported by RF President (grant no. MK-3771.2013.5); Russian Foundation for Basic Research (project no. 12-05-33032-a); and RF Ministry of Education and Science (projects nos. 8699, 8388 and contract no. 14.518.11.7065).

REFERENCES

Akhmedov, R.R. and Kunitsyn, V.E., Simulation of the ionospheric disturbances caused by earthquakes and explosions, *Geomagn. Aeron.*, 2004, vol. 44, pp. 95–101.

Bidlingmayer, E.R., Ivanovsky, A.I., and Pogoreltsev, A.I., Formation of the vertical structure of acoustic gravity waves by the molecular viscosity and thermal conductivity processes, *Izv. Akad. Nauk SSSR, Fiz. Atmos. Okeana*, 1990, vol. 26, no. 7, pp. 682–692.

Bidlingmayer, E.R. and Pogoreltsev, A.I., Numerical simulation of acoustic gravity wave transformation into temperature and viscous waves in the thermosphere, *Izv. Akad. Nauk SSSR, Fiz. Atmos. Okeana*, 1992, vol. 28, no. 1, pp. 64–73.

Fleming, E.L., Chandra, S., Schoeberl, M.R., and Barnett, J.J., *Monthly mean global climatology of temperature, wind, geopotential height and pressure for 0–120 km*, Washington: Nat. Aeronaut. Space Admin., 1988.

Gavrilov, N.M., Propagation of internal gravity waves in the stratified atmosphere, *Izv. Akad. Nauk SSSR, Fiz. Atmos. Okeana*, 1985, vol. 21, no. 9, pp. 921–927.

Gavrilov, N.M. and Yudin, V.A., Numerical study of the vertical structure of internal gravity waves from tropospheric sources, *Izv. Akad. Nauk SSSR, Fiz. Atmos. Okeana*, 1986, vol. 22, no. 6, pp. 563–571.

Gossard, E. and Hooke, W., *Waves in the atmosphere*, Amsterdam: Elsevier, 1975. Translated under the title *Volny v atmosphere*, Moscow: Mir, 1978.

Grachev, A.I., Zagoruiko, S.V., Matveev, A.K., Mordukhovich, M.I., and Chunchuzov, E.P., On atmospheric internal gravity waves from the source of the jet stream type, *Polyarn. Siyaniya Svechenie Nochnogo Neba*, 1981, no. 29, pp. 80–83.

Hedin, A.E., Extension of MSIS thermosphere model into the middle and lower atmosphere, *J. Geophys. Res.*, 1991, vol. 96A, pp. 1159–1172.

Hedin, A.E., Biondi, M.A., Burnside, R.G., et al., Revised global model of thermosphere winds using satellite and ground-based observations, *J. Geophys. Res.*, 1991, vol. 96A, pp. 7657–7688.

Ivanovsky, A.I. and Semenovsky, Yu.V., To the problem of the upper boundary conditions of the atmospheric tide theory, *Tr. TsAO*, 1973, no. 115, pp. 35–53.

Krasovsky, V.I., Potapov, B.P., Semenov, A.I., Sobolev, V.G., Shagaev, M.V., and Shefov, N.N., Internal gravity waves near the mesopause. I. Results of studies of the hydroxyl emission, *Polyarn. Siyaniya Svechenie Nochnogo Neba*, 1978, no. 26, pp. 5–29.

Kunitsyn, V.E., Suraev, S.N., and Akhmedov, R.R., Modeling the propagation of acoustic gravity waves in the atmosphere for different surface sources, *Vestn. Mosk. Univ., Ser. 3: Fiz. Astron.*, 2007, no. 2, pp. 59–63.

Landau, L.D. and Lifshits, E.M., *Gidrodinamika* (Hydrodynamics), Moscow: Nauka, 1978.

Pogoreltsev, A.I. and Pertsev, N.N., Effect of the background wind on the formation of the acoustic gravity wave structure in the thermosphere, *Izv. Akad. Nauk, Fiz. Atmos. Okeana*, 1995, vol. 31, no. 6, pp. 755–760.

Preusse, P., Eckermann, S.D., and Ern, M., Transparency of the atmosphere to short horizontal wavelength gravity waves, *J. Geophys. Res.*, 2008, vol. 113, p. D24104. doi 10.1029/2007JD009682

Shefov, N.N., Semenov, A.I., and Khomich, V.Yu., *Izluchenie verkhnei atmosfery - indikator ee struktury i dinamiki* (Emission of the upper atmosphere as an indicator of the atmospheric structure and dynamics), Moscow: GEOS, 2006.

Yanowitch, M., Effect of viscosity on gravity waves and the upper boundary condition, *J. Fluid Mech.*, 1967, vol. 29, pp. 209–231.

Translated by Yu. Safronov